In-Pixel Source Follower Transistor RTS Noise Behavior Under Ionizing Radiation in CMOS Image Sensors

Philippe Martin-Gonthier, *Member, IEEE*, Vincent Goiffon, *Member, IEEE*, and Pierre Magnan, *Member, IEEE*

***Abstract*—This paper presents temporal noise measurement results for several total ionizing dose (TID) steps up to 2.19 Mrad of an image sensor designed with a 0.18-μm CMOS image sensor process. The noise measurements are focused on the random telegraph signal (RTS) noise due to the in-pixel source follower transistor of the sensor readout chain inducing noisy pixels. Results show no significant RTS noise degradation up to 300 krad of TID. Beyond this TID step, a limited RTS noise degradation is observed, and for the 2.19-Mrad step, an additional increase of total noise, including thermal, 1/f, and RTS noises, is noted. Noisy pixels have been studied for high TIDs, and three cases have been observed: 1) no change on RTS behavior; 2) creation of RTS behavior; and 3) modifications of RTS behavior.**

***Index Terms*—Active-pixel sensor, CMOS image sensors (CISs), correlated double sampling (CDS), ionizing radiation, low-frequency noise (LFN), noisy pixels, random telegraph signal (RTS) noise.**

I. Introduction

NOWADAYS, CMOS image sensors (CISs) are extensively considered in commercial, scientific, and space applications [1]–[3]. The use of CIS processes has significantly enhanced their performances such as dark current (DC) and quantum efficiency [4]. In addition, the use of aggressive technologies and small in-pixel MOS transistors ($gate\ area < 1\ \mu\text{m}^2$) allows pixel photosensitive area improvement, leading to an increase of MOS transistor low-frequency noise (LFN) and particularly random telegraph signal (RTS) noise. The use of correlated double sampling (CDS) circuits and its associated readout mode allows elimination of photodiode reset noise which is usually the major noise contributor. At the same time, it reveals noisy pixels, coming from the in-pixel source follower (SF) transistor RTS noise, which becomes an issue for the low light sensitivity applications [3], [5].

LFN in large-area devices, showing a 1/f power spectral density, is well characterized by the use of appropriate models, known as McWhorter model [6], dealing with carrier number fluctuation; Hooge model [7], dealing with mobility fluctuation; or the unified model [8], dealing with carrier number fluctuation inducing mobility fluctuation.

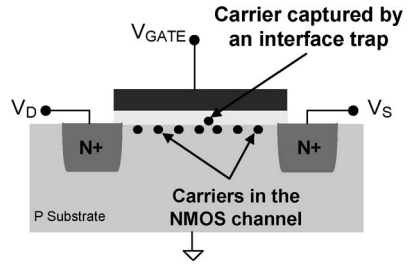

Fig. 1. Mechanism of carrier trapping/detrapping at Si/SiO_2 interface in small MOS transistor devices.

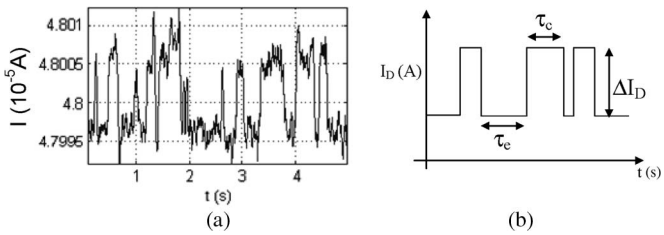

Fig. 2. RTS noise example coming from one defect at Si/SiO2 interface of a small MOSFET. (a) Measurements. (b) Model.

For small MOS transistor devices ($gate\ area < 1\ \mu\text{m}^2$), carrier number becomes small, and carriers in the transistor channel are captured and released by interface and near-oxide traps in contact with the channel, caused by individual interface defects at Si/SiO_2 interface, as shown in Fig. 1. The impact of trapping/detrapping events shows discrete drain current fluctuations [9].

Fig. 2(a) shows the measurements of this current fluctuation caused by one defect at Si/SiO2 interface for a small test MOS transistor. A two-level RTS noise appears. As can be seen in Fig. 2(b), three parameters can describe a two-level RTS noise: τ_e, the average carrier emission time; τ_c, the average carrier capture time; and ΔI_D, the drain current RTS amplitude depending on trap features [10].

The following equations depict these parameters, where ΔE_B is the trap energy level, ΔE_{CT} is the difference between energy levels of conduction band and trap, σ_0 is the trap capture cross section, x_T is the distance between the trap and Si/SiO2 interface, t_{OX} is the gate oxide thickness, T is the temperature, k is the *Boltzmann* constant, q is the elementary charge, I_D is the MOSFET drain current, g_m is the MOSFET transconductance, W and L are the MOSFET dimensions, C_{ox}

is the MOSFET gate oxide capacitance, and η and χ are the fabrication process constants [10]–[12]:

$$\tau_c = \frac{e^{\frac{\Delta E_B}{kT}}}{I_D T \sigma_0 \chi} \tag{1}$$

$$\tau_e = \frac{e^{\frac{\Delta E_B + \Delta E_{CT}}{kT}}}{T^2 \sigma_0 \eta} \tag{2}$$

$$\frac{\Delta I_D}{I_D} = \eta \frac{g_m}{I_D} . \frac{q}{W L C_{\mathrm{OX}}} . \left(1 - \frac{x_t}{t_{\mathrm{OX}}}\right). \tag{3}$$

An increase of the interface trap concentration at Si/SiO_2 interface under ionizing radiation is well established [13]. This increase induces LFN degradation in MOS transistor [14], leading to an increasing number of noisy pixels in CIS under ionizing radiation [15], [16]. Measurement results, shown in [15], from sensors exposed to X-ray radiations with total ionizing doses (TIDs) of 31 and 117 krad, show an important increase of noise at 117 krad. In [16], CISs were also irradiated with X-ray up to 250 krad. Measurements were only done up to 110 krad. Beyond this level, the sensor photon transfer curve was no longer acceptable for result analysis. Once again, at 110 krad, a noise degradation appears, explained by an RTS and 1/f noise increase. However, these noise results take into account the DC noise which participates to the total noise increase.

This paper presents noise measurements performed on a 3T-pixel test image sensor with a TID up to 2.19 Mrad. A specific readout sequence allows one to eliminate reset noise and to minimize integration time in order to make the DC noise negligible. The sensor output noise is shown for several TID steps (3 krad, 30 krad, 300 krad, 1 Mrad, and 2.19 Mrad). No significant noise variation is observed up to 300 krad. A noise variation is found beyond this TID, but safe images can be grabbed. The behavior of noisy pixels before and after radiations is depicted, showing different evolution cases.

II. Device Details and Preirradiation Results

The studied image sensor is a 10-μm-pitch 128 $\times$ 128 pixel array with 3T pixels manufactured using a 3.3-V commercial shallow trench isolation based 0.18-μm CIS process. The sensor architecture is shown in Fig. 3. This pixel is composed of a photodiode, a reset switch allowing reset of the photoelement, and an in-pixel SF which drives the signal from pixel to column readout circuit. This one consists of a double sample-and-hold circuit for reference and integrated signal level and an output stage allowing drive of the signal off chip or on chip for additional processing.

In order to study LFN and to remove reset noise from the 3T photodiode pixel (which is usually the major noise contributor), a specific readout sequence allowing CDS readout, shown in Fig. 4, is applied [17].

Compared to the common 3T photodiode readout sequence, reference and signal voltages are sampled in the same frame, leading to very short integration time (T_{INT}) that is equal to the CDS period. Due to the very small integration time, this readout sequence can only be used for noise characterization

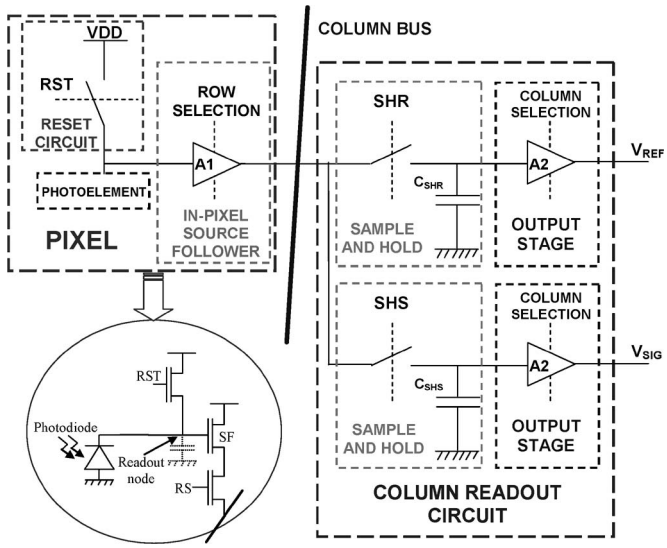

Fig. 3. Common architecture of a CIS.

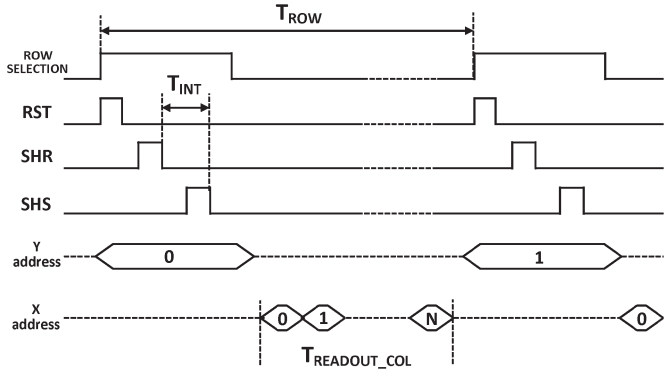

Fig. 4. Specific readout sequence allowing CDS readout with 3T pixel.

in darkness. This sequence allows the reset noise cancellation as for pinned photodiode (4T photodiode pixel). It also allows decreasing integration time close to 2 μs and hence minimizing photodiode DC inducing DC noise, which becomes negligible for the noise measurements [18].

Fig. 5 shows the cumulative histogram of the image sensor output noise obtained with the specific readout sequence before irradiation at 22 °C. The sensor mean output noise is around 194 μV rms. Noisy pixels are observed. Previous work [19] has clearly demonstrated the in-pixel SF RTS fluctuation impact on these noisy pixels.

The CDS principle requires two samples which are provided by the in-pixel SF transistor. If this transistor produces significant RTS noise, the pixel voltage response at the image sensor output shows different levels [17], [19]. Indeed, CDS acts as a filter, and the output signal can take different values, leading to multiple states of the temporal output signal histogram depending on the RTS level number. For example, Fig. 6 shows the temporal output signal histogram of a noisy pixel located at row #33 and column #18 (R33C18) of the image sensor, where three states can be seen.

Fig. 7(a) shows the output signal versus time of the same pixel (R33C18) measured directly, without CDS filtering. RTS

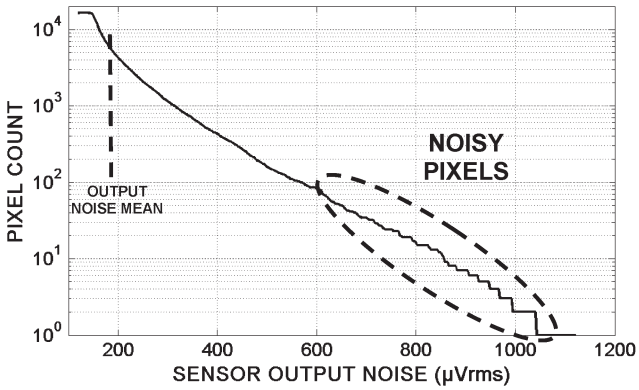

Fig. 5. Cumulative histogram of sensor output temporal noise at 22 °C.

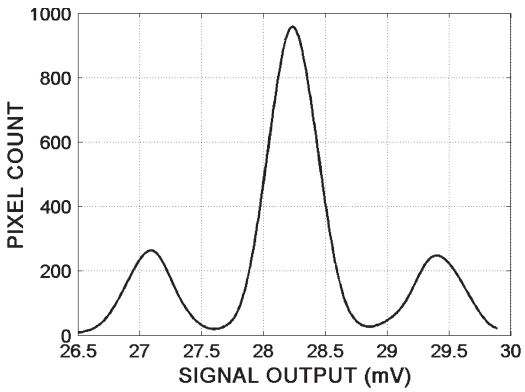

Fig. 6. Signal output histogram of pixel R33C18.

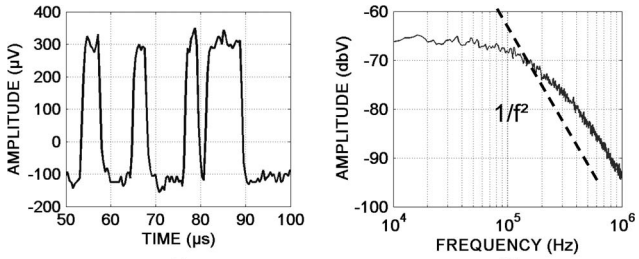

Fig. 7. R33C18 pixel. (a) Output signal versus time without CDS filtering. (b) Output signal spectrum showing a Lorentzian spectrum.

fluctuation is observed with two states. Fig. 7(b) shows the frequency spectrum in the bandwidth of the readout circuit. In the frequency domain, the output signal spectrum has the characteristics of a Lorentzian spectrum with a $1/f^1$ slope and a floor. It corresponds to a two-level RTS fluctuation [10].

III. Experimental Results After Irradiation

A ^{60}Co gamma ray source was used for irradiation. Radiation doses are given in rad. Noise measurements were done at several irradiation steps: 3 krad (SiO_2), 30 krad (SiO_2), 300 krad (SiO_2), 1 Mrad (SiO_2), and 2.19 Mrad (SiO_2). General measurements were performed and showed acceptable photon transfer curves allowing noise measurements.

Fig. 8 shows the pictures grabbed with the test image sensor read by a common 3T photodiode readout sequence without

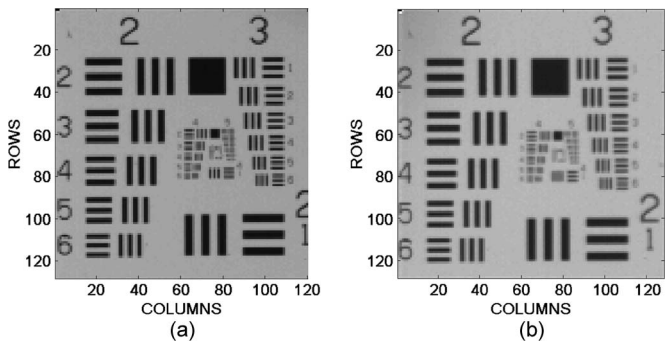

Fig. 8. Grabbed pictures of the test sensor with a common 3T readout sequence without CDS processing. (a) 1-Mrad TID. (b) 2.19-Mrad TID.

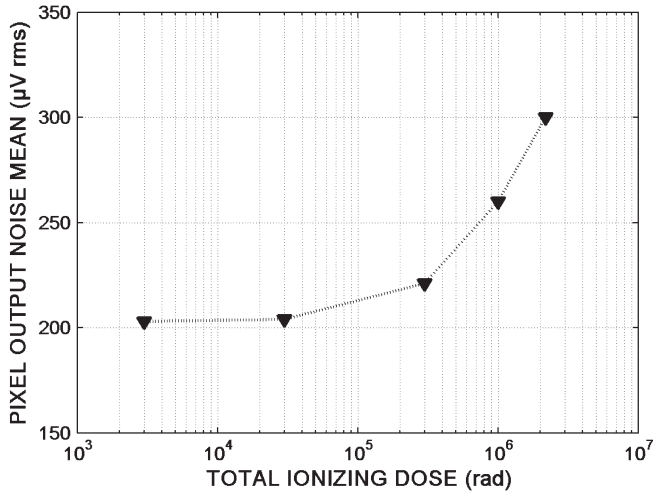

Fig. 9. Sensor mean output noise evolution versus TID.

CDS processing, leading to 35 ms of integration time at 1- and 2.19-Mrad TIDs. No major degradation is found in the picture except DC increase.

Noise measurements were done on the test image sensor with the specific readout sequence. Fig. 9 shows the evolution of sensor mean output noise versus TID. No significant noise increase can be seen up to 30 krad. Beyond this point, a noise degradation is observed, and an increase of 55% is reached at 2.19 Mrad.

The cumulative histogram of the sensor output noise gives more information about the noise degradation and particularly the noise behavior of the pixels (Fig. 10). Indeed, no significant changes are noted on sensor output noise shape up to 30 krad (no noisy pixel increase). For a 300-krad TID, an increase of noisy pixels is observed, which degrades the output noise mean. Up to 30 krad, only 34 pixels have an output sensor noise beyond 700 μV rms. At 2.19 Mrad, 96 pixels have an output sensor noise larger than 700 μV rms.

For the 1- and 2.19-Mrad TID cases, two facts can be noted. The first one concerns the increase of the noisy pixel number. The second one is the curve translation. Due to defect creation in oxide, two assumptions can explain this translation. First, the TID generates significant threshold voltage shift of the MOS transistor in the readout circuit, leading to a noise increase due to biasing changes [20], [21]. The other assumption concerns

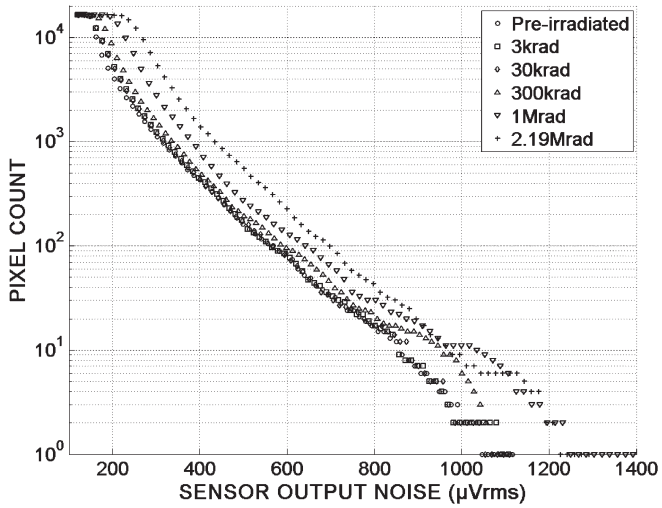

Fig. 10. Output sensor noise cumulative histogram for preirradiated, 3 krad, 30 krad, 300 krad, 1 Mrad, and 2.19 Mrad.

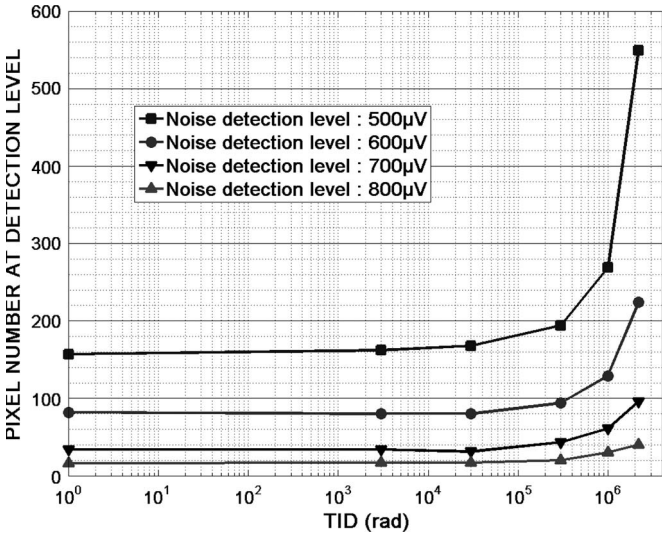

Fig. 11. Noisy pixel number versus TID for four noise detection levels: 500, 600, 700, and 800 μV rms.

the increase of LFN due to trap creation under irradiation, which impacts the noise of all pixels [21].

IV. Result Analysis and Discussion

Fig. 11 shows the increase of noisy pixel number versus the TID for several noise detection levels. For this graph, each pixel with a noise greater than the noise detection level is taken into account. As mentioned in the previous section, the number of noisy pixels increases for higher TID.

In order to study the noisy pixel behavior, each temporal histogram of noisy pixels, with a noise higher than 700 μV rms, was observed for the several TID steps. All these noisy pixels exhibit RTS behavior. Before irradiation, 34 noisy pixels are found with these criteria. After the 2.19-Mrad TID step, 96 noisy pixels are found (an increase of 182%). At this 2.19-Mrad TID step, pixels with noise exceeding 700 μV rms at readout chain output are selected, and their temporal output

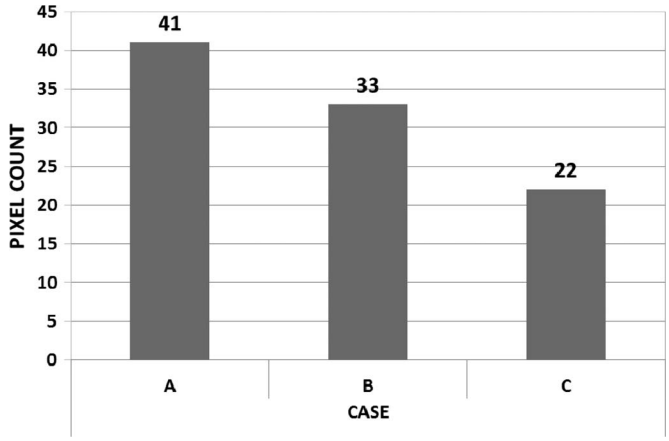

Fig. 12. Noisy pixel population segregation for the 2.19-Mrad TID step.

signal histograms are compared to the one before irradiation, leading to three cases. This segregation is shown in Fig. 12. These different populations correspond to the following.

1) Case A: Pixels before and after irradiation present RTS behavior, but peak locations on the temporal output histogram do not change; only peak values change.
2) Case B: Pixels before irradiation do not have RTS behavior, but after irradiation, pixels present RTS behavior.
3) Case C: Pixels before and after irradiation present RTS behavior, but peak locations and values on the temporal output histogram change.

No other cases for noisy pixel behavior, coming from these measurement results, have been observed for this circuit and these TID levels.

These three cases are described in the following sections.

A. No Change on RTS Behavior

This case is illustrated in Fig. 13 for the output signal histogram of the pixel located at row #25 and column #93 (R25C93) before irradiation and after a 2.19-Mrad TID. The 2.19-Mrad TID histogram peak values decrease, and states are spread compared to the values before irradiation.

This phenomenon can be easily explained by a first-order noise model. The following equation shows a signal which is the sum of a useful signal $s(t)$ and noise $\sigma(t)$:

$$\text{Signal}(t) = s(t) + \sigma(t). \tag{4}$$

The thermal noise from the readout chain $\sigma_{\text{TH\_READOUTCHAIN}}$ (Gaussian distribution) and LFN (in this case, RTS noise coming from in-pixel SF transistor $\sigma_{\text{RTS\_SF}}$) are considered uncorrelated, leading to

$$\sigma(t) = \sigma_{\text{TH}_{\text{READOUTCHAIN}}}(t) + \sigma_{\text{RTS\_SF}}(t). \tag{5}$$

Fig. 14 shows the qualitative simulation results for a given useful signal of 28 mV, a fixed in-pixel SF RTS noise (τ_e, τ_c, and ΔI_D, depending on the trap features), and different readout chain thermal noise values ($\sigma_{\text{TH_READOUT_CHAIN}} = 200\ \mu$V, 500 μV, and 1 mV).

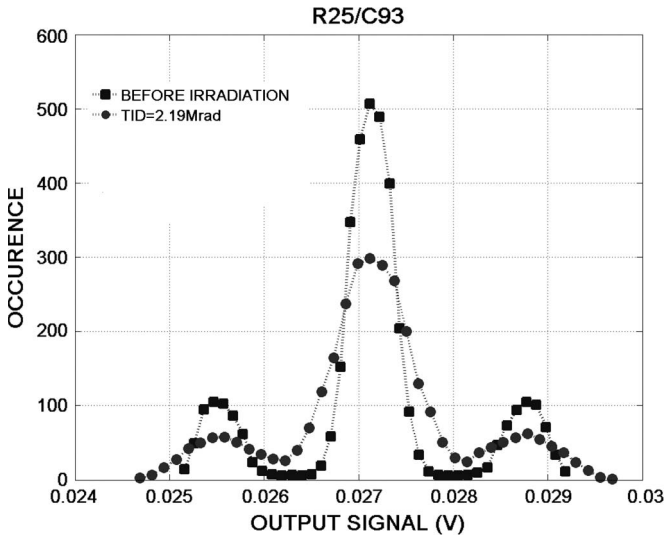

Fig. 13. Output signal histogram for the pixel R25C93 before irradiation and after a 2.19-Mrad TID.

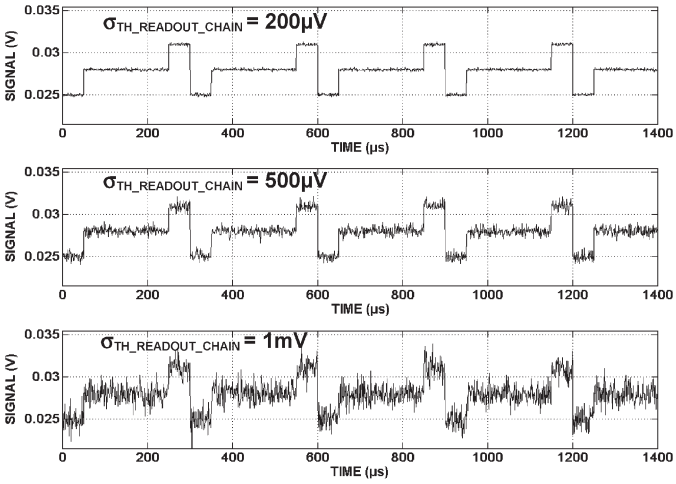

Fig. 14. Simulation results of signal(t) for a given SF RTS noise and three values of readout chain thermal noise with a useful signal.

Fig. 15 shows the signal histogram of this corresponding simulation. As for the measurement results, the histogram peak values decrease, and states are spread when readout chain thermal noise increases. This thermal noise increase is due to threshold voltage drift, coming from TID, leading to changes on readout chain biasing current [20], [21]. The measurement results and the first-order model demonstrate, in this case, that there is no change on the in-pixel SF RTS noise features.

B. RTS Pixel Creation

The second case is illustrated in Fig. 16 for the output signal histogram of the pixel located at row #32 and column #61 (R32C61) before irradiation and after a 2.19-Mrad TID. In this case, no RTS behavior is observed before irradiation. After a 2.19-Mrad TID, a histogram with three peaks, characteristic of in-pixel SF RTS behavior, appears.

The interface trap creation at Si/SiO_2 interface is well established under ionizing radiation [13]. In this case, only one trap

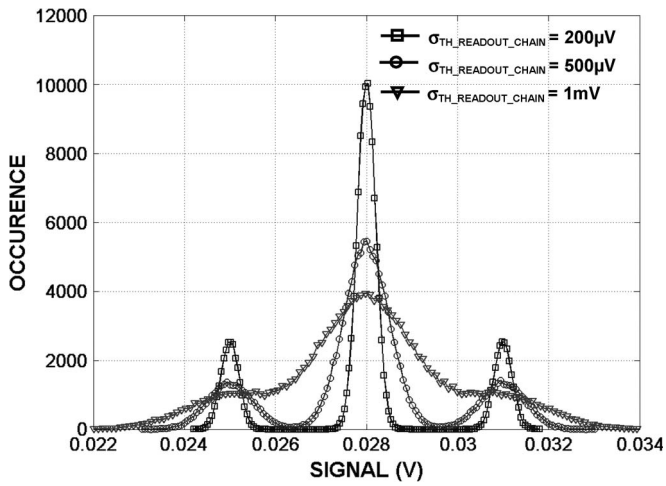

Fig. 15. Histogram of signal(t) from simulation results for a given SF RTS noise and three values of readout chain thermal noise with a useful signal.

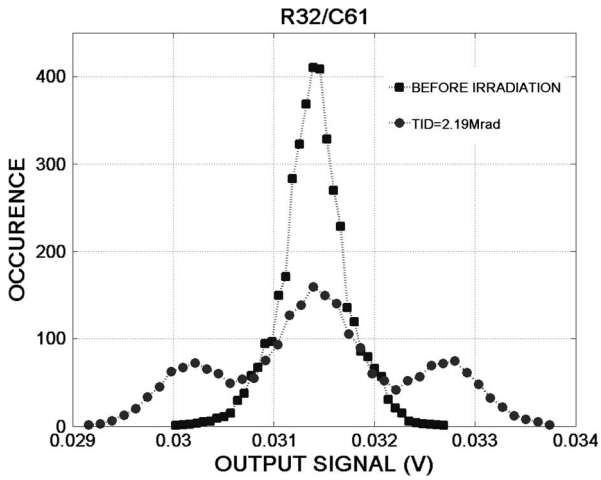

Fig. 16. Output signal histogram for the pixel R32C61 before irradiation and after a 2.19-Mrad TID.

is created at the Si/SiO_2 interface near the channel of the in-pixel SF inducing RTS behavior for a 2.19-Mrad TID. At the same time, an increase of thermal noise is observed, leading to a spread of the three peak values, as seen previously.

C. RTS Feature Modification

A third case of noisy pixel evolution after irradiation has been observed corresponding to a modification of the RTS behavior. Indeed, Fig. 17 shows the histogram of the pixel located at row #81 and column #1 (R81C1) before irradiation and for 300-krad and 1-Mrad TID steps. The two peaks due to in-pixel SF RTS behavior move away from the central peak, and peaks values decrease due to a signal value spread with irradiation increase.

This phenomenon can be modeled by the previous first-order noise model [(4) and (5)] with the thermal noise coming from the readout chain and the LFN (in this case, the RTS noise coming from the in-pixel SF transistor).

Fig. 18 shows the qualitative simulation results for a given DC signal of 28 mV; three different in-pixel SF RTS amplitudes

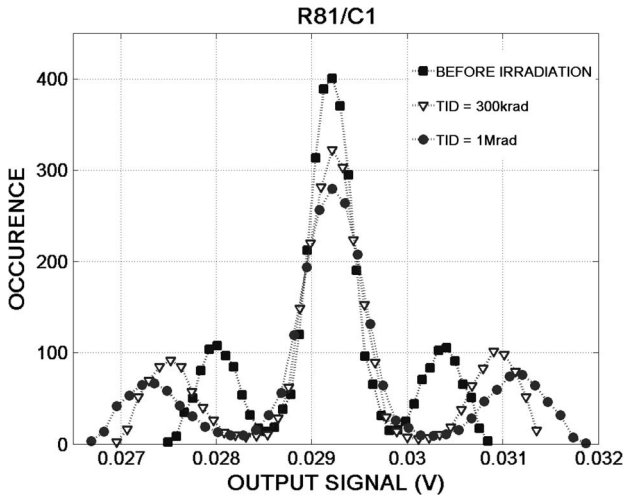

Fig. 17. Output signal histogram for the pixel R81C1 before irradiation and for 300-krad and 1-Mrad TID steps.

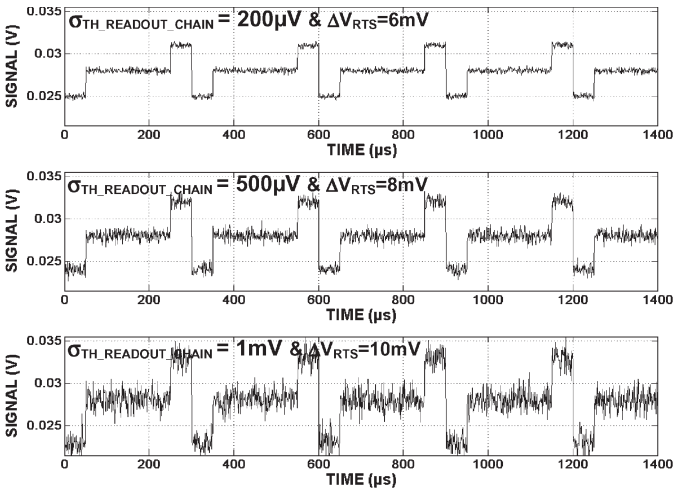

Fig. 18. Simulation results of $signal(t)$ for three different SF RTS amplitudes, leading to RTS noise, and three values of readout chain thermal noise with a useful signal.

($\Delta V_{\mathrm{RTS}} = 6$, 8, and 10 mV), leading to RTS noise; and different readout chain thermal noises ($\sigma_{\mathrm{TH\_READOUT\_CHAIN}} =$ 200 μV, 500 μV, and 1 mV).

Fig. 19 shows the signal histogram of this corresponding simulation. As for the measurement results, the two peaks due to in-pixel SF RTS behavior move away from the central peak, and peak values decrease with irradiation increase.

Signal value spread is explained by thermal noise increase with TID increase. Concerning the two peaks due to in-pixel SF RTS behavior, which move away from the central peak, RTS amplitude changes can be explained by the modification of the trap features. In this case, RTS amplitude grows with TID increase, leading to a noise increase. No other works mentioned this RTS behavior modification under irradiation. Further works are needed to find the impacted parameters.

In order to understand the global noise behavior, thermal and 1/f noises in one hand and RTS noise in the other hand should be segregated. Further works will be focused on this point to study the in-pixel SF transistor RTS noise under irradiation.

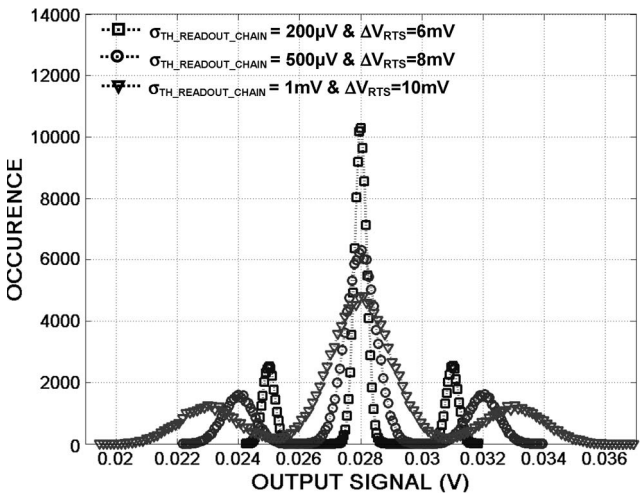

Fig. 19. Histogram of signal(t) from simulation results for three different SF RTS amplitudes, leading to RTS noise, and three values of readout chain thermal noise with a useful signal.

V. Conclusion

In this paper, noise measurement results for several TID steps, coming from an image sensor with a 10-μm-pitch 3T pixels based on a 0.18-μm CIS process, show no noise degradation up to 30 krad. At 300 krad, a limited increase of the number of noisy pixels due to in-pixel SF transistor RTS fluctuations is observed. At 2.19 Mrad, a degradation of thermal, 1/f, and RTS noises is noted, leading to a noisy pixel increase. Noisy pixels have been studied for high TIDs, and three cases have been observed: 1) no change on RTS behavior with only thermal noise increase; 2) creation of RTS behavior due to trap creation at the Si/SiO_2 interface near the channel of the in-pixel SF; and 3) modifications of RTS behavior due to trap feature alteration.

Acknowledgment

The authors would like to thank the CIMI Research Group, Institut Supérieur de l'Aéronautique et de l'Espace, Université de Toulouse, for the design and measurement support and particularly E. Havard, P. Cervantes, M. Estribeau, and G. Berger from the Université Catholique de Louvain for the irradiation facilities.

References

[1] E. R. Fossum, "CMOS image sensors: Electronic camera-on-a-chip," *IEEE Trans. Electron Devices*, vol. 44, no. 10, pp. 1689–1698, Oct. 1997.

[2] T. Lule, S. Benthien, H. Keller, F. Mutze, P. Rieve, K. Seibel, M. Sommer, and M. Bohm, "Sensitivity of CMOS based imagers and scaling perspectives," *IEEE Trans. Electron Devices*, vol. 47, no. 11, pp. 2110–2122, Nov. 2000.

[3] P. Martin-Gonthier, P. Magnan, F. Corbiere, S. Rolando, O. Saint-Pe, M. B. de Boisanger, and F. Larnaudie, "CMOS detectors for space applications: From R&D to operational program with large volume foundry," in *Proc. SPIE Sens., Syst., Next-Generation Satell. XIV*, 2010, p. 7826.

[4] M. Furumiya, H. Ohkubo, Y. Muramatsu, S. Kurosawa, F. Okamoto, Y. Fujimoto, and Y. Nakashiba, "High sensitivity and no-crosstalk pixel technology for embedded CMOS image sensor," *IEEE Trans. Electron Devices*, vol. 48, no. 10, pp. 2221–2227, Oct. 2001.

[5] K. Findlater, J. M. Vaillant, D. J. Baxter, C. Augier, D. Herault, R. K. Henderson, J. E. D. Hurwitz, L. A. Grant, and J.-M. Volle, "Source

follower noise limitations in CMOS active pixel sensors," in *Proc. SPIE Detect. Assoc. Signal Process.*, 2004, vol. 5251, pp. 187–195.
[6] A. L. Mc Whorter, " 1/f noise and germanium surface properties," in *Semiconductor H. Surface Physics*. Philadelphia, PA: Univ. of Pennsylvania Press, 1957.
[7] F. N. Hooge, " 1/f noise is no surface effect," *Phys. Lett.*, vol. 29, no. 3, pp. 139–140, Apr. 1969.
[8] K. Hung, P. Ko, C. Hu, and Y. Cheng, "A unified model for the flicker noise in metal–oxide–semiconductor field-effect transistors," *IEEE Trans. Electron Devices*, vol. 37, no. 3, pp. 654–665, Mar. 1990.
[9] C. Leyris, F. Martinez, M. Valenza, A. Hoffmann, J. C. Vildeuil, and F. Roy, "Impact of random telegraph signal in CMOS image sensors for low-light levels," in *Proc. 32nd ESSCIRC*, Sep. 2006, pp. 376–379.
[10] M. J. Kirton and M. Uren, "Noise in solid-state microstructures: A new perspective on individual defects, interface states and low-frequency (1/f) noise," *Adv. Phys.*, vol. 38, no. 4, pp. 367–468, Nov. 1989.
[11] E. Simoen, B. Dierickx, C. Claeys, and G. Declerck, "Explaining the amplitude of RTS noise in submicrometer MOSFETs," *IEEE Trans. Electron Devices*, vol. 39, no. 2, pp. 422–429, Feb. 1992.
[12] J. M. Woo, H. H. Park, S. M. Hong, I. Y. Chung, H. S. Min, and Y. J. Park, "Statistical noise analysis of CMOS image sensors in dark condition," *IEEE Trans. Electron Devices*, vol. 56, no. 11, pp. 2481–2488, Nov. 2009.
[13] T. P. Ma and P. V. Dressendorfer, *Ionizing Radiation Effects in MOS Devices and Circuits*. New York: Wiley-Interscience, 1989.
[14] D. M. Fleetwood, T. L. Meisenheimer, and J. H. Scofield, " 1/f noise and radiation effects in MOS devices," *IEEE Trans. Electron Devices*, vol. 41, no. 11, pp. 1953–1964, Nov. 1994.
[15] Y. Chen, J. Tan, X. Wang, A. J. Mierop, and A. J. P. Theuwissen, "In-pixel buried-channel source follower in CMOS image sensors exposed to X-ray radiation," in *Proc. IEEE Sensors*, Nov. 1–4, 2010, pp. 1649–1652.
[16] R. E. Coath, J. P. Crooks, A. Godbeer, M. D. Wilson, Z. Zhang, M. Stanitzki, M. Tyndel, and R. A. D. Turchetta, "A low noise pixel architecture for scientific CMOS monolithic active pixel sensors," *IEEE Trans. Nucl. Sci.*, vol. 57, no. 5, pp. 2490–2496, Oct. 2010.
[17] P. Martin-Gonthier and P. Magnan, "Novel readout circuit architecture for CMOS image sensors minimizing RTS noise," *IEEE Electron Device Lett.*, vol. 32, no. 6, pp. 776–778, Jun. 2011.
[18] V. Goiffon, P. Magnan, P. Martin-Gonthier, C. Virmontois, and M. Gaillardin, "Evidence of a novel source of random telegraph signal in CMOS image sensors," *IEEE Electron Device Lett.*, vol. 32, no. 6, pp. 773–775, Jun. 2011.
[19] X. Wang, P. R. Rao, A. J. Mierop, and A. J. P. Theuwissen, "Random telegraph signal in CMOS image sensor pixels," in *Proc. IEDM*, Dec. 11–13, 2006, pp. 1–4.
[20] T. R. Oldham and F. B. McLean, "Total ionizing dose effects in MOS oxides and devices," *IEEE Trans. Nucl. Sci.*, vol. 50, no. 3, pp. 483–499, Jun. 2003.
[21] M. Gaillardin, V. Goiffon, S. Girard, M. Martinez, P. Magnan, and P. Paillet, "Enhanced radiation-induced narrow channel effects in commercial 0.18 μm bulk technology," *IEEE Trans. Nucl. Sci.*, vol. 58, no. 6, pp. 2807–2815, Dec. 2011.

Philippe Martin-Gonthier (M'09) was born in Jonzac, France, in 1973. He received the M.S. degree in electrical engineering from ENSERB, Bordeaux, France, in 1998, the Diplôme d'Etudes Approfondies degree in integrated circuit design from ENSAE, Toulouse, France, in 2001, and the Ph.D. degree in electrical engineering from the Université de Toulouse, Toulouse, in 2010. His doctoral research focused on noise in submicrometer CMOS sensors and design techniques.

Since 1998, he has been a Scientist with the Image Sensor Research Team, Institut Supérieur de l'Aéronautique et de l'Espace, Université de Toulouse. His research interests include solid-state image sensors, integrated circuit design, noise, and particularly random telegraph signal in pixel arrays.

Vincent Goiffon (S'08–M'09) was born in Toulouse, France, in 1980. He received the M.S. degree in electrical engineering and the M.S. degree in aeronautics and astronautics from SUPAERO, now called Institut Supérieur de l'Aéronautique et de l'Espace (ISAE), Université de Toulouse, Toulouse, both in 2005 and the Ph.D. degree in electrical engineering from the Université de Toulouse in 2008. His doctoral research, partly funded by CNES and EADS Astrium, focused on space radiation effects on deep submicrometer CMOS sensors and hardening-by-design techniques.

Since 2008, he has been an Associate Professor with the Image Sensor Research Team, ISAE, Université de Toulouse. His research interests include solid-state image sensors, integrated circuit design, dark current, device TCAD modeling and simulation, semiconductor defect characterization, ionization and displacement damage effects, and random telegraph signal in pixel arrays.

Pierre Magnan (M'99) was born in Nevers, France, in 1958. He received the M.S. and Diplôme d'Etudes Approfondies degrees in integrated circuit design from the University of Paris XI, Orsay, France, in 1982 and the Agregation degree in electrical engineering from the Ecole Normale Supérieure de Cachan, Cachan, France.

From 1984 to 1993, he was with LAAS, CNRS, Toulouse, France, where he was involved in CMOS analog and semicustom design. In 1995, he joined the CMOS Imagers Research Group, SUPAERO, Toulouse, where he was involved in active-pixel sensor research and development activities. In 2002, he got his Accreditation for Ph.D. Supervision (H.D.R) and became Full Professor at SUPAERO, now called Institut Supérieur de l'Aéronautique et de l'Espace, where he is currently the Head of CMOS Imagers Research Group. He has been supervising 8 Ph.D. candidates in the field of image sensors and has authored or coauthored 30 papers and a patent. His research interests include solid-state image sensor design, modeling, technology, and integrated circuit design for imaging applications.

Prof. Magnan is a member of the Program Committee of the International Image Sensor Workshop in 2007 and 2009.